CORONAL OSCILLATIONS IN THE VICINITY OF A SUNSPOT AS OBSERVED BY GIS/CDS

C.H. Lin[1], D. Banerjee[2], J.G. Doyle[1], E. O'Shea[1]

[1]*Armagh Observatory, College Hill, Armagh BT61 9DG, N. Ireland*

[2]*Indian Institute of Astrophysics, Koramangala, Bangalore 560034, India*

ABSTRACT

We present the analysis and results of GIS (Grazing Incidence Spectrometer) time series observed on 19th July 2003 at the boundary between the quiet Sun and an active region, close to a sunspot. The velocity map of NIS/CDS O V 629 Å shows two pairs of red and blue shifts surrounding the brightest region. Presumably, we have observed coronal loops with opposite flow velocities. Although our observations were not taken directly at the sunspot, the 3-min oscillations are seen in several coronal spectral lines. Thus the coronal loops can have some connection with the sunspot, in the vicinity. We report here of oscillations in these coronal loops as observed with coronal lines formed around 1 MK or higher. Furthermore, the oscillations form wavepackets and are intermittent with no obvious decay. The average time scale of the intermittence is of the order of 20 minutes.

1. INTRODUCTION

The detection of oscillations in coronal loops is critical in determining the presence of waves in the corona and their relevance to the problem of coronal heating. The oscillations in the atmosphere directly above various solar features have been extensively investigated by a range of instruments. Fludra (1999, 2001) investigated 3 min intensity oscillations above sunspots with CDS. He concluded that the 3 min umbral oscillations can occur both in the so called sunspot plumes (bright features seen in the transition region above a sunspot) and in the lower intensity plasma closely adjacent to the plumes. SUMER observations (in both intensity and velocity) have confirmed that the sunspot oscillations are prominent in transition region lines above the umbra (Maltby et al. 2001). Brynildsen et al. (1999a,b; 2004) observed oscillations in intensity and velocity, and found the oscillations to be compatible with the hypothesis of upwardly propagating waves. More recently, O'Shea et al. (2002) and Brynildsen et al. (2002, 2004) have both presented joint observations of the 3 min umbral oscillations with TRACE and CDS. Banerjee et al. (2002) detected both intensity and velocity oscillations in chromospheric and transition region lines as observed by CDS. They have shown that the 3 minute intensity and velocity oscillations are a property of the umbra, and not just the sunspot plume.

In contrast to the extensive study of sunspots, there has been little attention paid to the study of oscillations in the vicinity of a sunspot. In this paper, we present the analysis and results of an observation pointed at the boundary between the quiet Sun and an active region, corresponding to coronal loops faning out of a sunspot.

2. THE OBSERVATION AND DATA

Our data was obtained with the Grazing Incidence Spectrometer (GIS), which is one of the two components of the Coronal Diagnostic Spectrometer (CDS), on board the Solar Heliospheric Observatory. A more detailed description of the GIS instrument can be found in e.g., Harrison (1995) and the CDS Web-page.

The GIS sequence analyzed in this paper was taken as part of a Sunspot/Active region study on July 19, 2003. The observation was a 90-minute sit-and-stare operation pointed in the southern heliosphere. The solar rotation rate at this latitude implies a coverage of approximately 11″of the solar surface. The GIS signal is a one-dimensional time series without spatial resolution (astigmatic). To determine the location of the observation and to examine the features we are observing, we incorporated the information from TRACE, NIS/CDS and MDI images. To correct for the coordinate offsets between different instruments, we chose NIS coordinates as the standard coordinates, and shifted the images of other instruments until the features matched the features in the NIS image.

Fig. 1 shows a global view of the entire active region under discussion as seen with the 171 Å TRACE wavelength band. The contours represent the distribution of magnetic field as recorded by MDI. The small black rectangular box overlayed on these images at around location $513'' < X < 524''$, $Y \approx -218''$denotes our determined field of view (FOV) of GIS, with a pointing accuracy of $\approx 5''$. From a comparison of the magnetic contours and the position of the rectangular box, one can conclude that in the GIS FOV, no significant magnetic fields/structures are present at the photosphere level. We are, however, at the boundary between an active region and the "quiet Sun".

2.1 Data reduction

GIS data were calibrated and corrected for instrumental effects using routines from the Solar Software library. The data was first converted from FITS format to a Quick Look Data Structure (QLDS) by `readcdsfits`, and the wavelengths were calibrated through `restore wavecal` and `pix2wave`. Next, the two main instrumental errors, "fixed patterning",

Proceedings of the SOHO 15 Workshop - Coronal Heating, St. Andrews, Scotland, 6-9 September 2004
(ESA SP-575, December 2004)

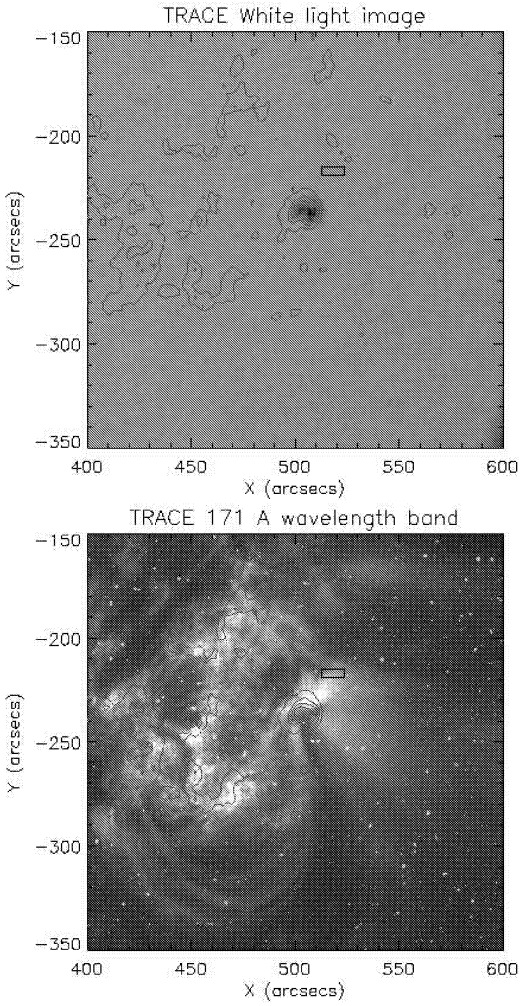

Figure 1. An overview of the region of our observation at different temperatures. TRACE white light and TRACE 171 Å channel ($\log T_e = 5.9$*). The contours in the images represent the MDI magnetogram. The rectangular box represents our region of observations with GIS.*

caused by electronic read-out errors, and "ghosting", an effect when the intensities of certain lines are partially shifted and recorded in a wrong spectral region, are reduced by `gis_smooth` and `ghost_buster`, respectively (See Del Zanna, 1999 for details on GIS "ghosting"). Finally, the `gis_calib` procedure corrects the electronic effects on line intensities. The unit of the intensity is converted into counts. (see CDS Software note No. 55 for the details of the errors and the calibration of GIS data)

The fitting of spectral lines was performed through `xcfit` and `xcfit_block`. The fitted lines that show large fluctuations in line widths and/or positions were discarded. Table 1 lists all the lines selected for our further analysis. The temperature of ionization equilibrium of each line was calculated from CHIANTI synthetic spectra, `ch_ss`, using `mazzotta_etal_ext.ioneq` as

Table 1. The fitted lines

The selected spectral lines		
Element	wavelength	log T_{eff}
Fe XV	284	6.3
Fe XI	188	6.1
Fe IX	171	5.9
Ne VIII	770	5.9
Ne VIII	780	5.9
Ca IX	466	5.8
Ne VII	465	5.8
N IV	765	5.1
He II	304	4.9

the ionization fractions file and `active_region.dem` as the differential emission measure file. After the fitting, the total intensity of each selected spectral line was then computed. The oscillations were extracted by subtracting the trend from the intensity. The errors in the oscillation amplitudes are computed based on CDS Software Note No. 49. The top panel in Fig. 3 is an example of the oscillations and the associated errors.

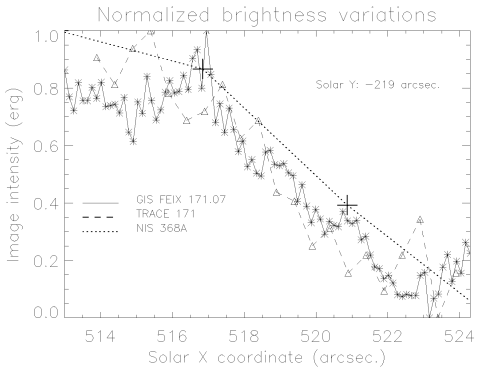

Figure 2. The light curve of GIS Fe IX *171 Å and the brightness variations in the TRACE 171 Å band and NIS Mg* IX *368 Å line for a region 514″<X<525″, Y≈ −219″. The symbols mark the actual data points (as labelled) .*

NIS and TRACE images were calibrated, using standard calibration routines (see O'Shea et al. 2002 for further details). The offset between NIS1 and NIS2 was corrected using the routine `nis_rotate`. However, no calibration was applied to MDI images.

Details on the wavelet analysis may be found in *e.g.*, Torrence & Compo (1998) and O'Shea et al. (2001). Fig. 3 illustrates one example of the wavelet transform on the oscillations. The multiple peaks in the global wavelet spectrum (the center right panel) in the example are due to the fact that the signals are often composed of oscillations of different periods. To examine the features and properties of the oscillation of a specific period, it is thus necessary to apply a bandpass filter to the signal. In our

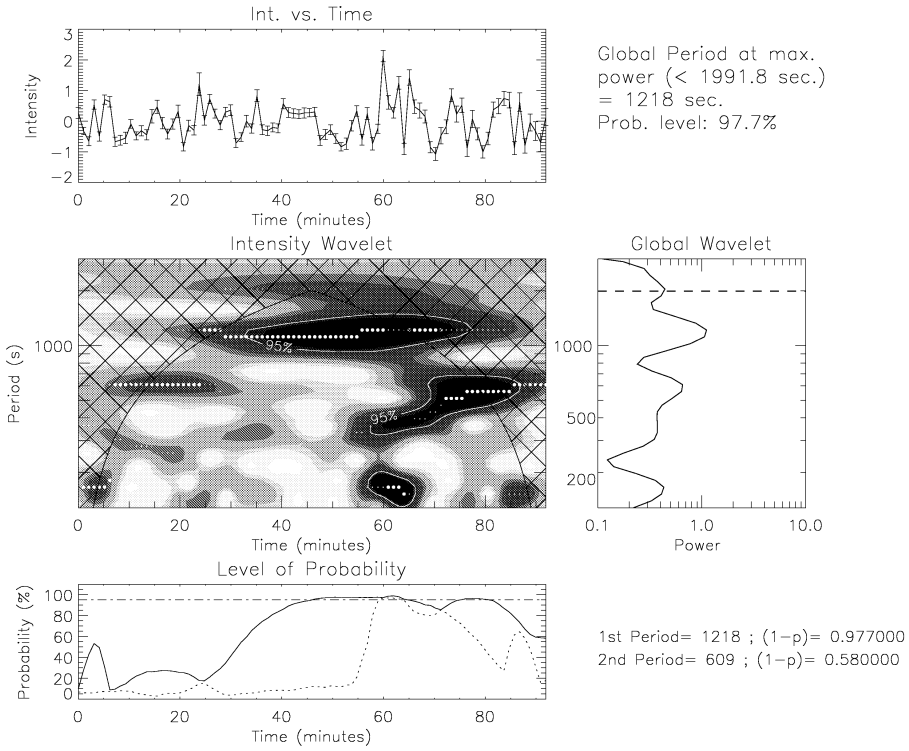

Figure 3. One example of the wavelet analysis on the intensity variations (after subtracting the trend). Fe IX *171 (*$\log T_e = 5.9$*). The error bars represent computed intensity errors based on CDS Software Note No. 49.*

analysis, we implemented three passbands: [0 – 250]second, [250 – 500]second and [500 – 900]second, which are to extract 3-min, 5-min. and 10-min. oscillations, respectively.

3. RESULTS AND DISCUSSION

Fig. 2 compares the normalized GIS Fe IX 171 Å light curve with the normalized brightness variations in the TRACE 171 Å band and the NIS Mg IX 368 Å line in the region $514'' < X < 525''$and $Y \approx -218''$. The close resemblance of the variations to one another confirms that we have been able to correct the off-set between different instruments and to correctly determine the FOV of the GIS observation. In Fig. 3, we show a typical example of oscillations as recorded by the Fe IX 171 Å line. The top panel shows the original intensity variations (after subtracting the trend) in counts/s along with the errors. In the wavelet spectrum (the middle left panel), the dark contour regions show the locations of the highest power. The light white horizontal lines within the dark contour regions indicate the locations of the maximum wavelet power at each particular time. The lowest panel shows the variation of the probability level over the observing time, by which it is possible to see whether the maximum wavelet power at any time in the wavelet spectrum has a high or low probability of being due to noise. Only locations that have a probability greater than 95% are regarded as being real, *i.e* not due to noise. Cross-hatched regions, on either side of the wavelet spectrum, indicate the 'cone of influence' (COI), where edge effects become important (see Torrence & Compo, 1998). The dashed horizontal lines in the wavelet spectra (middle right panel) indicates the higher period cut-off, in this instance 1991.8s (due to edge effects). One can see that there are multiple peaks as revealed by the global wavelet spectra, indicating the presence of more than one period. In Fig. 4, we show our region of observations as seen in NIS O V 629 Å and the velocity map of the region. The contours represent the distribution of magnetic field as recorded by MDI and the small rectangular box represents the GIS FOV. The arrows indicate the locations at which a completely new $4'' \times 4''$area enters the field of view of the GIS slit. From the NIS O V 629 Å image, we can see a region of strong emission (the brightening) which overlaps the sunspot (compare the O V image in Fig. 4 and the upper panel in Fig. 1). The velocity map of NIS O V shows two pairs of red and blue shifts surrounding the brightening. The Doppler velocity computed from the red shifts is approximately 40 km/sec and the velocity from blue shifts is less than 30 km/sec. Such magnitude indicates that the shifts are likely due to the flows in the loops. The boundary of the upper red and blue shifts is the region of our GIS observation. After a closer inspection of the velocity map and the other images, we suggest that our GIS observation was obtained at the crossing of loops with opposite

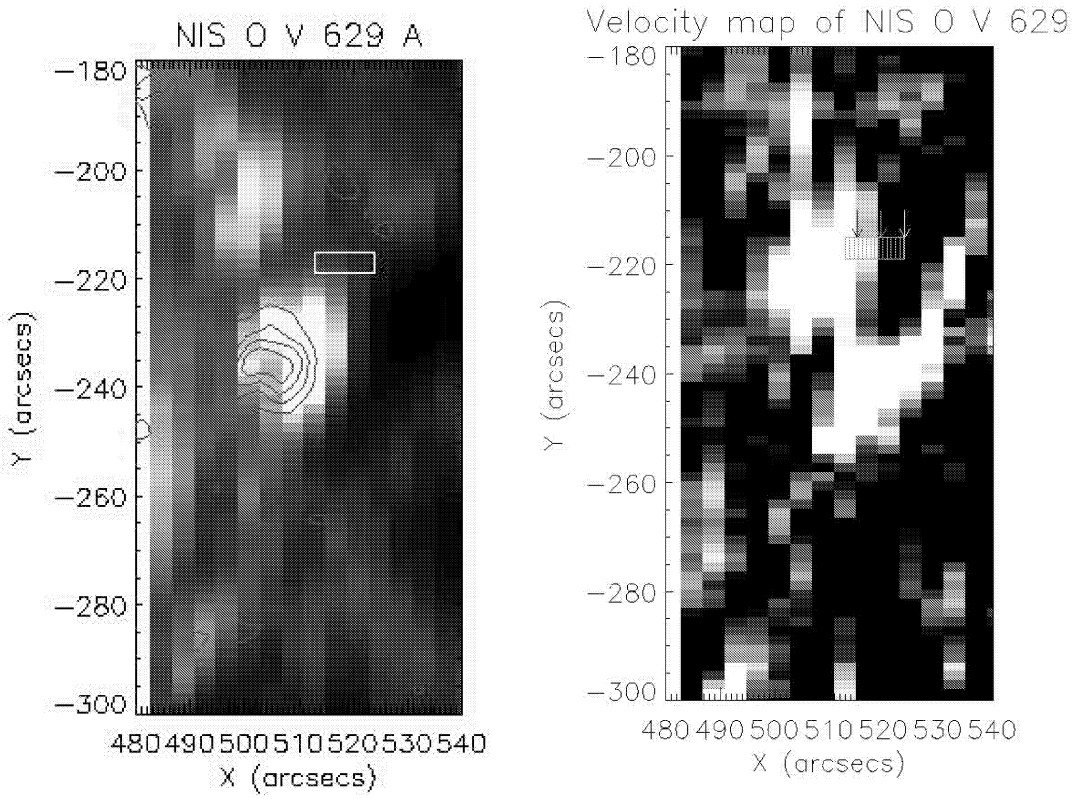

Figure 4. The left panel shows the region of our observation seen in a NIS O V *intensity map. The contours represent magnetic field concentrations as revealed by a MDI magnetogram. The rectangular box indicates the FOV of the entire GIS observation. The right panel shows the velocity map of NIS O* V*. The excess red shifts are represented by bright colours. The lines, within the rectangular box mark the time steps, and the arrows above the rectangular box indicate the locations at which a completely new 4″ × 4″ area enters the field of view of the GIS slit.*

Table 2. The selected lines and their oscillation periods

Line (Å)	Temp. ($\log T_e$)	0–250 second		250–500 second		500–900 second	
		period (sec.)	Prob. level (%)	period (sec.)	Prob. level (%)	period (sec.)	Prob. level (%)
Fe XV 284	6.3	181	96.5	332	99 – 100	609	99 – 100
Fe XI 188	6.1	166	92.5	394	99.5	664	99 – 100
Fe IX 171	5.9	166	96.5	362	99 – 100	609	99 – 100
Ne VIII 770	5.9	181	97	332	99 – 100	789	99 – 100
N IV 765	5.1	166	78.0	469	99 – 100	939	99 – 100

flow directions.

3.1 The oscillations

Among the lines we studied, we present here the results of those that are strong and free from blending. Table 2 is a synopsis of the oscillations of these lines. The table shows that the probability level of the 3-min. oscillation is above 90% in most lines, except for N IV 765, which is a transition region line.

Fig. 5 shows an example of the filtered oscillations and wavelet spectra of the three passbands. We should point out here that the 3-min. oscillations (*i.e.,* [0 – 250] passband) in N IV 765 Å , formed at $\log\ T_e = 5.1$, is significantly weaker than oscillations in the other two passbands. Significant oscillations of this line are for periods of 5 min. and higher.

There are several intriguing characteristics that are common in all of our oscillations:

1. The period and amplitude of the oscillations vary over the 90-minute observation. This could also be due to sit and stare effect (note that the GIS FOV re-

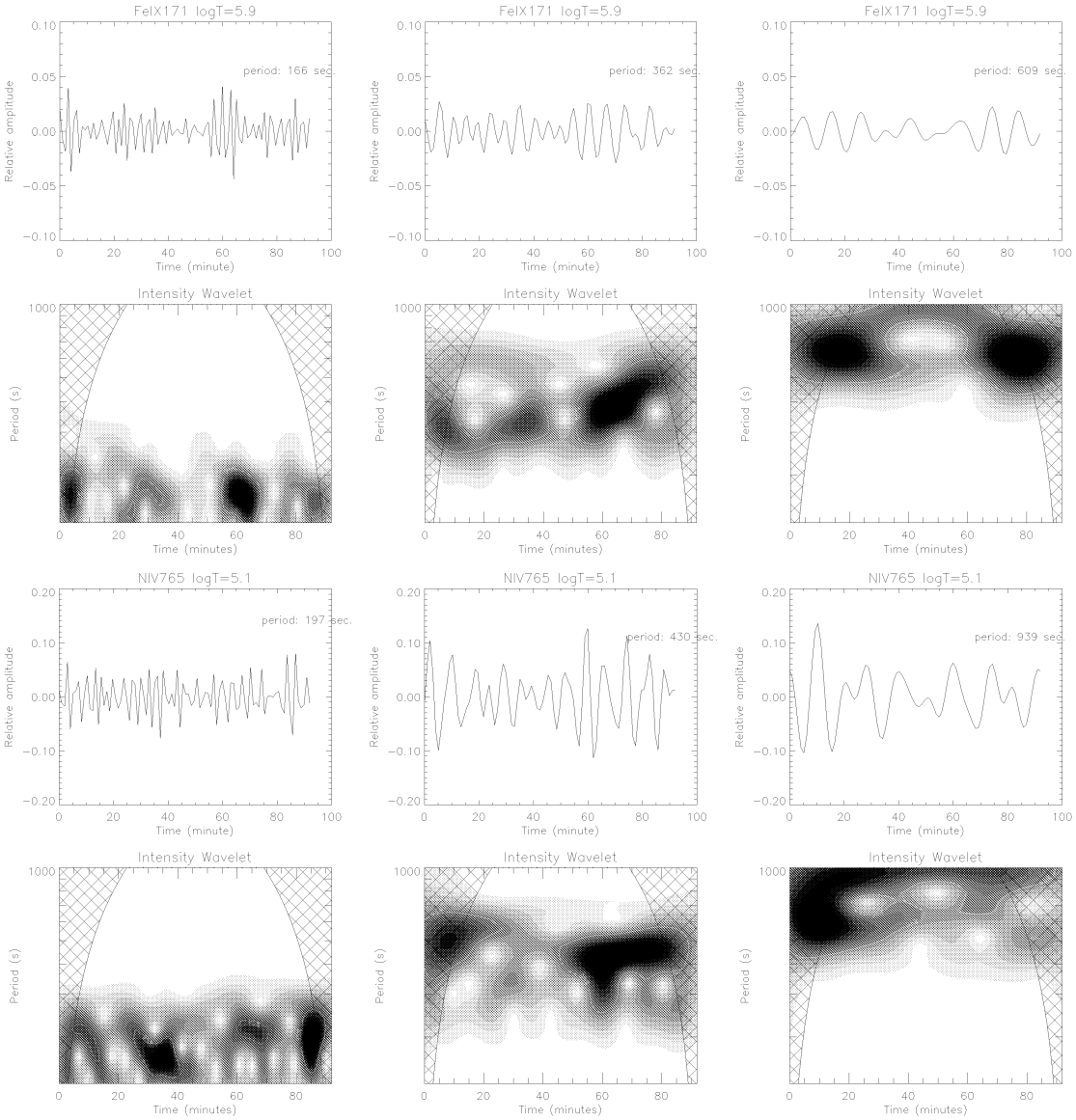

Figure 5. Filtered oscillations and wavelet spectra. The upper two rows correspond to Fe IX *171, and the lower two rows N* IV *765. The passband of each column, from left to right, is [0 – 250], [250 – 500] and [500 – 900].*

mains same only for 36 minutes). Thus, unless the spatial coherence of these oscillations are of the order of 10 arc sec or more, we do not expect to see the same oscillations for the entire observing period.

2. Although our observation is not directly above the sunspot, the 3-min. oscillations, which heretofore have been considered to exist only in the umbra, are seen in all of our selected lines except for the aforementioned N IV line. It could well be that our coronal loops are somehow connected with the sunspot in the vicinity.

3. The oscillations are intermittent and wavepacket-like with no obvious decay. Such intermittency, although appearing in all lines, is more prominent in the hot lines ($\log T_e > 5.8$, *e.g.,* Fe IX) than in cool lines ($\log T_e < 5.8$, *e.g.,* N IV). The average time scale of the intermittence is of the order of 20 minutes.

4. The 10-min. oscillations, corresponding to the [500 – 900] passband, are clean and prominent in all the lines we examined. The uniformly high level of significance of these oscillations (cf. Table 2) is a result of their long durations. The oscillations last longer than 40 minutes without decay in many lines. However, their periods and amplitudes do vary over that time.

GIS detectors detect the integrated light intensity over a $4'' \times 4''$area. As the Sun rotates, new areas would gradually enter the field of view of the slit of the detector. Due to the solar rotation rate at the latitude of our observation,

the slit would cover a completely new $4'' \times 4''$region every 36 minutes. In Fig. 4, the arrows in the velocity map indicate these locations. If our determined region of observation is correct within the pointing accuracy, the slit would begin to detect the region of red shift after the 24th minute and would be completely in the red-shift region after the 60th minute. The boundary of blue/red shift would dominate the field of view from the 36th to 48th minute. We believe that we have a scenario in which the slit crosses two system of loops with opposite flows. We try to find an effect of this transition from the power spectra. We found that most of the lines we analyzed do not exhibit obvious change at these locations. Ne VIII 770 and Fe XV 284 show slightly stronger oscillations in the blue-shift zone than in the red-shift zone. However, such slight difference is not significant.

3.2 Summary

Although the intermittency is common in all the oscillations, it is more prominent in hot lines than in cool lines. We found that the locations where a wavepacket starts and stops do not show an apparent correlation with temperature variation, and are not always associated with the locations of the red/blue-shift boundary and the red/blue-shift zones. The lack of correlation between the oscillations and the variations in temperature could indicate that the loops are inclined or twisted, or that the thermal structures in the loops are not stratified. The indifference of the blue/red shifts, an indication of flow, to the oscillations suggests that the oscillations are not affected by the flow.

4. CONCLUSIONS

In our present observation we have a complicated topology. It is very difficult to conclude from the available data that the loops we observe have direct links with the dominant sunspot in the vicinity. De Moortel et al. (2002) pointed out that loops that are situated above sunspot regions display intensity oscillations with periods of the order of 172 ± 32 seconds, whereas oscillations in non-sunspot loops show periods of the order of 321 ± 74 secs. In our observation we find both the 3-min and 5-min periodicity in addition to the prominent 10-min oscillations. However, the 3-min oscillations in our results are often isolated oscillations, with a duration of ≈ 20 minutes. In addition, our results show that in the region of our observation 3-min oscillations are relatively stronger in hotter lines than in cooler lines.

We must point out that our observations suffer from the sit and stare effect, thus probably we are observing different loops at different times. Taking into account all the observed properties we can interpret our observed oscillations as propagating slow magnetoacoustic waves, which are not easily damped. Furthermore, our observation indicates that the drivers are probably near the footpoints and definitely not flare driven.

ACKNOWLEDGEMENTS

We would like to thank the CDS and EIT teams at Goddard Space Flight Center for their help in obtaining the present data and Carl Foley for his help with the GIS data. CDS and EIT are part of SoHO, the Solar and Heliospheric Observatory, which is a mission of international cooperation between ESA and NASA. DB wishes to thank the Royal Society London and the DST, India. His visit to the Armagh Observatory was supported within the India-UK Science Networks program. Research at Armagh Observatory is grant-aided by the N. Ireland Dept. of Culture, Arts and Leisure. This work was supported by a PRTLI research grant for Grid-enabled Computational Physics of Natural Phenomena (Cosmogrid). The original wavelet software was provided by C. Torrence and G. Compo, and is available at URL: http://paos.colorado.edu/research/wavelets/.

REFERENCES

Banerjee, D., O'Shea, E., Goossens, M., Doyle, J. G., Poedts, S., 2002, A&A, 395, 263B

Brynildsen, N., Leifsen, T., Kjeldseth-Moe, O., Maltby, P., Wilhelm, K., 1999a, ApJ, 511, L121

Brynildsen, Kjeldseth-Moe, O., Maltby, P., Wilhelm, K., 1999b, ApJ, 517, L159

Brynildsen, N., Maltby, P., Fredvik, T., Kjeldseth-Moe, O., 2002, Sol Phys, 207, 259

Brynildsen, N., Maltby, P., Foley, C., Fredvik, T., Kjeldseth-Moe, O., 2004, Sol Phys, 221, 237

De Moortel, I., Ireland, J., Hood, A. W., Walsh, R. W., 2002, A&A, 387, L13

Del Zanna, G., 1999, Ph.D dissertation

Fludra, A. 1999, A&A, 344, L75

Fludra, A. 2001, A&A, 368, 639

Harrison, et al. 1995, Sol. Phys., 162, 233

Maltby, P., Brynildsen, N., Kjeldseth-Moe, O., Wilhelm, K., 2001, A&A, 373, L1

O'Shea, E., Banerjee, D., Doyle, J.G., Fleck, B., Murtagh, F. 2001, A&A, 368, 1095

O'Shea, E., Muglach, K., Fleck, B., 2002, A&A, 387, 642

Torrence, C., & Compo, G.P. 1998, Bull. Amer. Meteor. Soc., 79, 61